Absolute cross sections for proton-induced fission of the uranium isotopes

J. R. Boyce,* T. D. Hayward,† R. Bass,‡ H. W. Newson, E. G. Bilpuch, and F. O. Purser
Triangle Universities Nuclear Laboratory, Duke University, Durham, N.C. 27706§

H. W. Schmitt
Oak Ridge National Laboratory, Oak Ridge, Tennessee 37830¶
(Received 25 February 1974)

Absolute cross sections for proton induced fission have been measured for ^{233}U, ^{234}U, ^{235}U, ^{236}U, and ^{238}U for proton energies ranging from 5.0 to 30.0 MeV. Angular distributions have been measured for all isotopes and the fission fragment angular anisotropy determined as a function of excitation energy. Excitation data were accumulated at 250 keV intervals with smaller steps in regions of special interest. Fission probabilities calculated from the data and optical model predictions prominently display effects due to the opening of additional fission channels as excitation energy is increased. A method of analysis is formulated and demonstrated which makes use of the extended energy range and selection of an isotopic sequence of target nuclei to unfold the contributions to the measured cross section from first, second, and third chance fission. Using this method, previously undetermined fission thresholds and Γ_n/Γ_f ratios are estimated for individual nuclei as functions of excitation energy.

[NUCLEAR REACTIONS, FISSION ^{233}U(p,xnf), ^{234}U(p,xnf), ^{235}U(p,xnf), ^{236}U(p,xnf), and ^{238}U(p,xnf), $E=5.0$–30.0 MeV; measured $\sigma_{p,xnf}(E_p,\theta)$; deduced $\sigma_{fT}(E)$, $\Gamma_n/\Gamma_f(E,A)$, fission barriers.]

I. INTRODUCTION

The experimental study of the fission process at higher excitation energies is complicated usually by the presence of several fissioning nuclei. At energies well above the (p,n) or the (n,n') threshold, neutron evaporation competes quite strongly with fission and, when the residual nucleus after neutron emission can itself fission, these fission events are usually indistinguishable from those caused by fission decay of the initial compound nucleus. For very moderate excitation energies (on the order of 35 MeV for the actinide nuclei) as many as five different nuclei along the neutron decay chain may contribute to the usual fission measurement; details of the fission process for individual fissioning nuclei are therefore obscured. This is particularly true, of course, if the experiment seeks information concerning a quantity such as the mass division which is excitation energy dependent, since the different nuclei contributing to the measurement are at quite different average excitation energies.

Previously reported measurements of proton induced fission cross sections for uranium include those of Fulmer,[1] Choppin, Meriwether, and Fox,[2] and Bate and Huizenga.[3] More recently, Baba, Umezawa, and Baba[4] have reported a study of ^{238}U for proton energies from 13 to 55 MeV in which the total fission cross section is deduced from measured mass yields. A recent paper by Bishop *et al.*[5] reports work in which the energy dependence of the fissionability and the branching ratio Γ_n/Γ_f for neutron evaporation and fission were investigated by measurements of post-fission and pre-fission neutrons. In this latter work, which extended to a proton energy of 22 MeV, the analysis includes provision for the presence of yields from first, second, and third chance fission events of ^{239}Np.

The present paper reports a series of cross section measurements for proton induced fission of five uranium isotopes with initial excitation energies ranging from 10 to 37 MeV. Data for a series of targets of adjacent mass number and for an extended energy range permit an attempt to unfold the individual contributions of the multiple chance fission process occurring in the measurement. The initial analysis reported here utilizes simple Bohr-Wheeler[6] parabolic fission barriers, the Gilbert and Cameron[7] level density formalism and straightforward statistical model assumptions concerning the decay of the compound nucleus. The results of this analysis include the Γ_n/Γ_f ratios for the neptunium isotopes and experimental values for several previously unreported thresholds.

II. EXPERIMENTAL

A. Procedure

The experiments were performed at Triangle Universities Nuclear Laboratory (TUNL) using the proton beam from the FN tandem accelerator for energies below 16 MeV and using the Cyclo-Graaff accelerator for higher energies. The direct beam from these accelerators was analyzed by two 90° bending magnets with a designed resolving power, $\Delta E/E$, of 1.26×10^{-4}. Beam energy spread at the targets was never more than 10 keV at the highest energies measured and ranged downward for the lower energies.

The geometry of the target chamber is shown in Fig. 1. The incident beam was tightly collimated at the chamber entrance by a series of circular tantalum apertures with the smallest aperture having a diameter of $2\frac{1}{4}$ mm. Fission fragments were detected by ORTEC 400 mm^2 heavy ion detectors cooled to dry ice temperature. Detector to target distances were set to an accuracy of ± 0.05 mm using machined distance gauges. Detector solid angles for fission fragments were determined by 0.127 mm thick Mylar collimators. An additional 1.52 mm thick tantalum collimator was used to prevent spurious pulses due to the high energy proton interactions in the nonuniform detector edge regions.

Beam currents on target were varied from 30 to 400 nA to limit counting rates to prescribed levels free of electronic dead time effects. Since beam integration is a critical factor in absolute cross section determinations, particular attention was paid to obtaining accurate charge accumulation. Beam current was integrated using a Brookhaven integrator with an input impedance of less than 5×10^{-6} Ω. This integrator was calibrated at the beginning of each extended data run and the calibration was periodically rechecked during the runs. The Faraday cup was well isolated with an electrical resistance to ground greater than 10^{12} Ω and both the Faraday cup and the target were positively biased to suppress emission of secondary electrons. Test runs, with differing beam current levels and running times which varied by factors of 10, produced cross section results which fluctuated statistically about the mean observed value and indicated no systematic variation with beam current level or running time. Suppression of secondaries was also tested by installing a 1500 G magnet at the Faraday cup entrance. Repeated runs with and without magnetic suppression produced identical results, and for most of the data the magnet was not used.

Uranium targets were supplied by Oak Ridge National Laboratory on either 20 μg/cm^2 carbon or 50 μg/cm^2 nickel backings. Target thicknesses and isotopic constitution are given in Table I. The method by which target thicknesses were determined is discussed in the next section.

Relative fission yields at a laboratory angle of 90° were measured at 250 keV or smaller intervals. During each extended run, yields at normalization energies of 10, 11, 12, and 13 MeV were measured and rechecked at intervals to

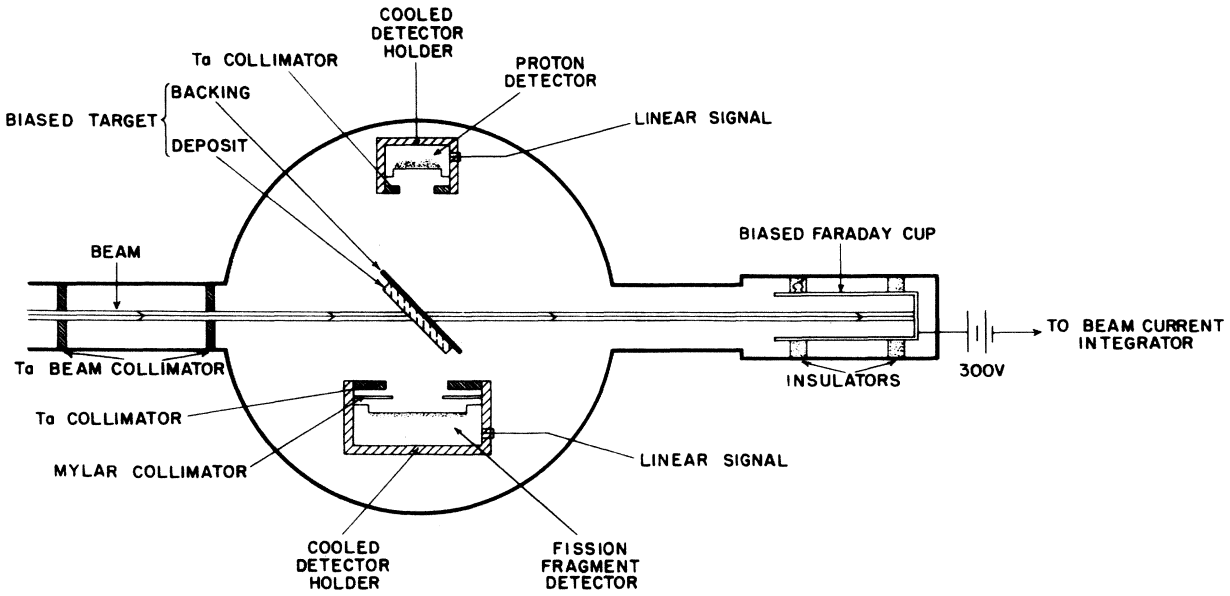

FIG. 1. A schematic diagram of the target chamber arrangement for the 90° cross section measurements.

ensure that any target erosion by the beam could be detected. For ^{235}U an additional check was obtained by measuring the initial yield curve in ascending 500 keV steps to the highest energy point. Intermediate points were then measured in descending 500 keV steps to the lowest energy point and were found to be consistent with the original curve over the entire energy range. A summary of the experimental uncertainties is given in Table II.

A final check on the accuracy of the yield curve data was made by repeating most of the measurements over a period of several months. In every case, the data were reproducible to within the accuracy quoted.

The fission fragment angular distributions were measured in a 60 cm diam scattering chamber to allow larger target to detector distances and a greater angular range. Two detectors were placed 180° apart at equal distances from the target. Target to detector distances and solid angles were set as described for the 90° yield curves. Angular acceptance of the detectors used was 2.5° in the reaction plane. Measurements were made at 10° intervals from 20 to 100° (lab) with one detector and simultaneously from 160 to 80° (lab) with the other. The overlapping points at 80, 90, and 100° were used to normalize the detectors to each other to eliminate the very small difference between the two detector solid angles. This symmetric arrangement minimizes any experimental effects due to beam spot wander.

TABLE I. Target characteristics. Method of measurement: a: Coulomb scattering of 10.0 MeV α particles; b: Coulomb scattering of 5.0 MeV protons; c: The 5 MeV proton data corrected for contaminant.

Target (backing)	Batch composition A	(%)	Thickness at 45° ($\mu g/cm^2$) a	b	c
^{233}U (carbon)	233	99.998	78.80 ±0.74	82.64 ±0.53	80.20 ±0.74
	234	<0.001			
	235	<0.001			
	236	<0.001			
	238	<0.001			
^{234}U (nickel)	233	0.038	101.48 ±1.80	107.79 ±0.91	102.28 ±0.95
	234	99.420			
	235	0.303			
	236	0.077			
	238	0.162			
^{235}U (carbon)	233	<0.701	72.34 ±0.42	78.69 ±0.28	74.66 ±0.97
	234	<0.739			
	235	99.440			
	236	0.454			
	238	0.067			
^{236}U (nickel)	233	0.010	139.72 ±0.95	147.06 ±1.35	139.70 ±1.21
	234	0.001			
	235	0.199			
	236	99.680			
	238	0.110			
^{238}U (carbon)	233	<0.01	25.25 ±0.20	25.00 ±0.34	25.00 ±0.29
	234	<0.01			
	235	<0.01			
	236	<0.01			
	238	>99.90			

B. Target thickness measurements

Target thicknesses were determined by measuring Rutherford scattering angular distributions. Initial target thickness values obtained from Rutherford scattering of 5 MeV protons resulted in fission cross sections which were somewhat inconsistent with previously reported work and were, moreover, nonsystematic from isotope to isotope. Investigation of the targets with a 10 MeV α particle beam revealed the presence in the uranium targets of varying amounts of a high Z contaminant, most probably tungsten. Protons scattered from this contaminant were kinematically unseparable from the uranium elastic peak in the proton pulse height spectra and therefore had contributed to the proton Rutherford scattering data. With the α beam, at the scattering angles used and with the detector and electronic resolution obtained, any contaminant lighter than lead was separable.

Following the discovery of the target contaminant the relative fission yields were converted to absolute cross sections by the following procedure:
(i) The targets were installed in the scattering chamber with both a particle detector and a fission fragment detector.
(ii) A Rutherford scattering angular distribution was measured using 10 MeV α particles. For each point in the distribution a uranium target

TABLE II. Experimental uncertainties.

Uncertainty	Target ^{233}U (%)	^{234}U (%)	^{235}U (%)	^{236}U (%)	^{238}U (%)
Statistical [a]	1.00	1.00	1.00	1.00	1.00
Beam integration	0.50	0.50	0.50	0.50	0.50
Target thickness	0.93	1.93	1.30	1.87	1.20
Solid angle	1.00	1.00	1.00	1.00	1.00
Normalization	0.50	0.50	0.50	0.50	0.50
Anisotropy	<0.50	<0.50	<0.50	<0.50	<0.50
Total uncertainty	1.90	2.54	2.11	2.50	2.05

[a] The statistical uncertainty of 1% was arbitrarily set for the number of events, N_e, when $N_e > 10000$. When $N_e < 10000$ the uncertainty used was $\sqrt{N_e}$.

thickness and a contaminant yield were determined.
(iii) Without changing target position or detector geometry a 5 MeV proton beam was brought into the chamber and a proton Rutherford scattering angular distribution measured.
(iv) Proton beam energy was increased and 90° fission yields were measured at 10, 11, 12, and 13 MeV with sufficient precision to render the statistical uncertainty of each point insignificant.
(v) Contaminant yields determined by the α particle measurements were used to determine the true uranium elastic scattering yields in the proton Rutherford scattering distribution. New target thicknesses were then calculated for each angle in the proton Rutherford angular distribution. The rms average of these target thickness results agreed well with the α particle measurements and was used to reduce the fission yield data to absolute cross sections. The accurately determined reference cross sections at 10, 11, 12, and 13 MeV were used as normalization points to which all yield curve data were normalized.

Target thicknesses quoted in Table I are the result of a rms combination of the results at each angle of the Rutherford measurements. Errors quoted do not include the possible deviations due to target nonuniformity. Two of the targets used for the ^{234}U and ^{236}U data were slightly wedge shaped being thicker on one edge than the other. While the beam spot was tightly collimated to reduce the effects of any such nonuniformity, the uncertainties quoted for the cross section data for these two isotopes have been increased to reflect this possible source of error.

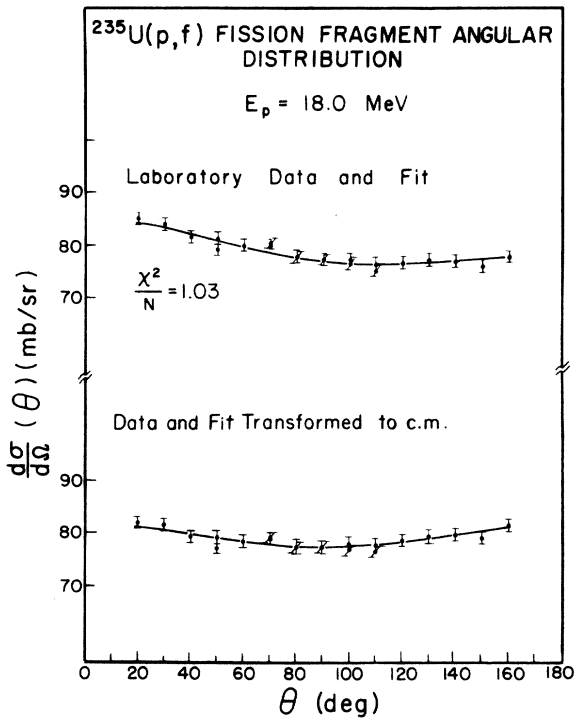

FIG. 2. A typical fission fragment angular distribution shown for both the laboratory and center of mass transforms.

III. CROSS SECTION RESULTS

In order to obtain total fission cross sections the fission fragment angular anisotropy as a function of energy is required. Over 100 eighteen point angular distributions were measured at regular energy intervals in the energy range covered by the 90° yield data. A typical angular distribution is shown in Fig. 2. Each angular distribution was transformed to the center of mass and then fitted by an exact least squares with a sum of even Legendre polynomials: $W(\theta) = \sum_0^3 a_{2n} P_{2n}(\cos\theta)$. Only the coefficients of P_0 and P_2 were statistically nonzero so that the distributions have at most a $\cos^2\theta$ dependence. The distributions were then fitted to the more common form assumed for fission fragment angular distribution analysis: $W(\theta) = (1 + \epsilon \cos^2\theta)$. The results of this analysis are shown in Fig. 3 where the anisotropy coefficient ϵ is plotted as a function of beam energy. The smooth line represents only a visual fit through these data. A more detailed analysis of these angular distribution data will be presented in a forthcoming paper.

Figure 4 shows the differential cross sections for the five uranium targets. In this figure the data contain a scale factor f which allows adequate visual separation.

The total experimental fission cross section for each isotope was then obtained by

$$\sigma_F = \int \sigma(\theta) d\Omega = 4\pi(1 + \tfrac{1}{3}\epsilon)\sigma(90°). \quad (1)$$

The values of ϵ used were taken from the smooth lines in Fig. 3. Since the anisotropy is only a small correction to the total cross section the values used may differ somewhat from the true values without affecting the cross sections appreciably. When plotted on a semilog scale the total cross section data show the characteristics of other charged particle induced fission cross sections. At low energies the behavior is dominated by Coulomb barrier penetration, whereas at higher energies the fission cross section approaches the total reaction cross section. Tabulations of the total fission cross section data for the five target isotopes are available at TUNL.

The effect of the Coulomb penetrability can be removed in a manner similar to the ratio-to-

Rutherford technique used to remove Coulomb scattering effects in ordinary charged particle angular distributions. Since Coulomb penetrability effects are included in reaction cross sections calculated with the optical model, these effects in the data can be largely removed by dividing the measured cross sections by the calculated reaction cross sections. If the reaction cross section calculated with the optical model is a true compound nuclear formation cross section, the result obtained will be the total fission probability of the initial compound nucleus. The calculation of the compound nucleus formation cross section is outlined in the next section.

The results of these calculations are shown in Fig. 5. The fission probabilities σ_F/σ_r show a step structure similar to that observed in neutron induced fission where the observed steps can be correlated with the onset of second, third, or even higher chance fission.

IV. DATA ANALYSIS

A. Introduction

An idealized multiple chance fission process is shown in Fig. 6(a) in an excitation versus mass number plane. Here the primary compound system ^{237}Np is formed by bombardment of 27 MeV

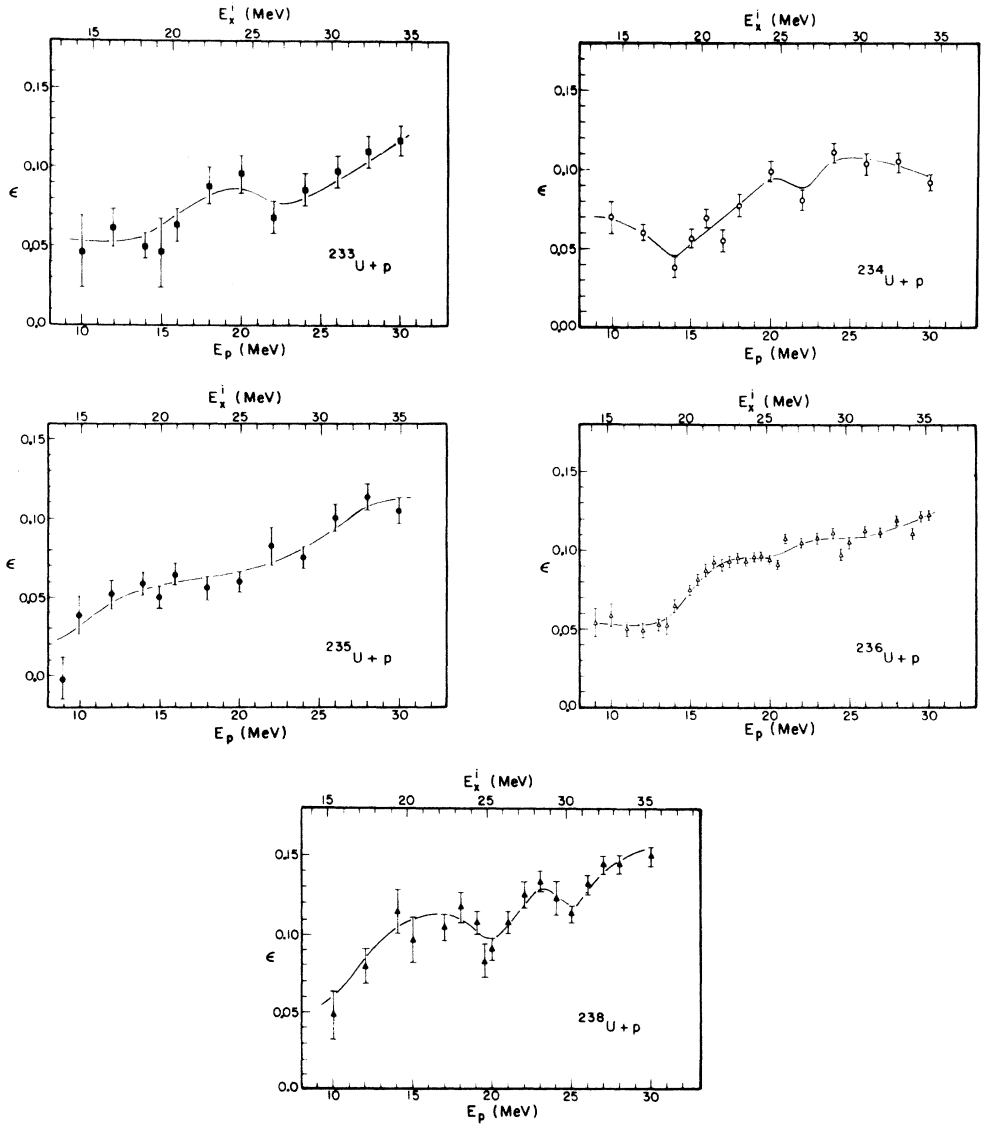

FIG. 3. The angular anisotropies obtained from the fission fragment angular distributions. The upper scale for each graph is the excitation energy in the initial compound nucleus. Curves shown indicate the anisotropies used to obtain total cross sections from the 90° (lab) yields. As shown, the measured anisotropies are quite small.

protons on ^{236}U. From this primary compound system a sequence of lighter Np isotopes can be reached by successive neutron evaporations, and each of these can decay again either by neutron evaporation or by fission. In this idealized example a neutron evaporates with fixed energy such that the excitation energy of the residual nucleus is 6 MeV less than that of the parent nucleus. The sequence is terminated either by fission or by arrival at an excitation energy below the fission barrier and the neutron binding energy.

The consequences for the measured fission cross section for this special case are shown in Fig. 6(b), which gives the total fission probability P_f, defined as the ratio of the fission cross section to the compound nucleus formation cross section, as a function of incident proton energy. This example assumes the same decay width for both neutron and fission channels. The steps in P_f occur at the various (p, xnf) thresholds in complete analogy to the well known behavior of excitation functions for fast neutron induced fission.

To a first approximation two types of information can be obtained from such probability curves: the fission thresholds $E_f(A)$, and the branching ratios Γ_n/Γ_f. The former can be deduced from the onset of the additional fission chance exhibited by the increase of P_f at the beginning of the associated step. The branching ratios can be obtained from the level of the step providing the assumption is made that the ratio is slowly varying with energy for excitation energies well above the fission threshold.

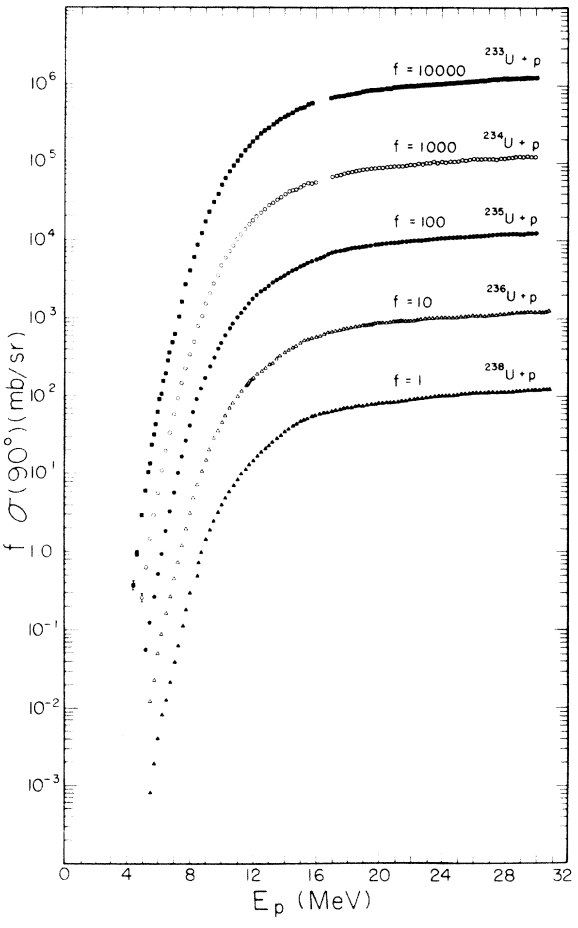

FIG. 4. The differential cross sections at 90° (lab). The ordinate has been expanded by a factor f to allow visual separation of the data. The effect of the angular anisotropy is so minor that this figure (with a scale change) could also represent the total fission cross sections.

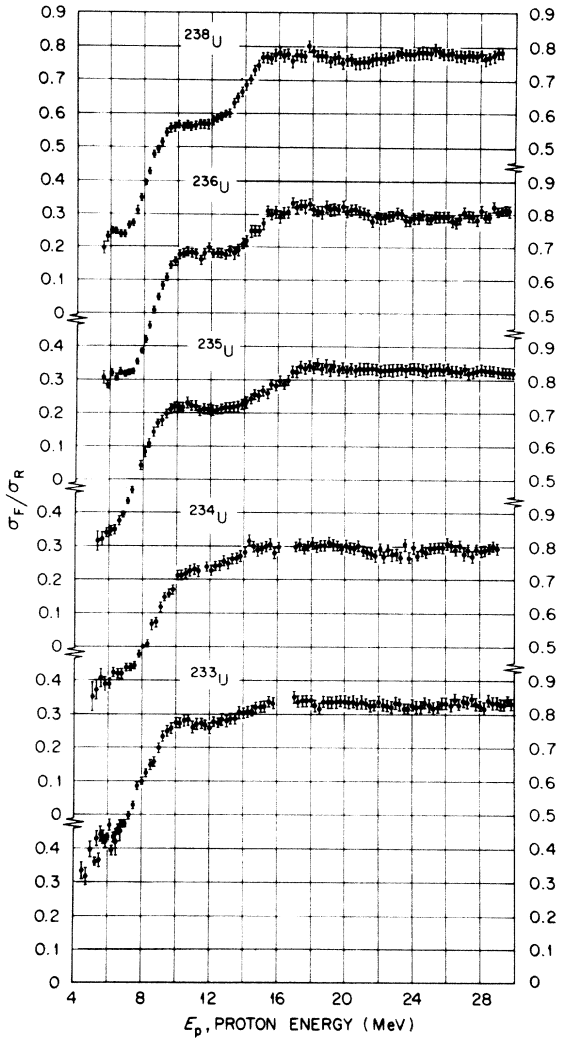

FIG. 5. Approximate total fission probabilities for the five target isotopes as a function of proton energy. The reaction cross section used was obtained from the published parameters of Becchetti and Greenlees (Ref. 8).

This manner of obtaining information concerning the properties of a nucleus must yield self-consistent results. That is, the fission threshold $E_f(A)$ deduced from the onset of second chance in $P_f(A+1)$ must agree with that obtained from the onset of third chance in $P_f(A+2)$. Similarly, the branching ratios Γ_n/Γ_f for nucleus (A) deduced from the first chance plateau in $P_f(A)$ must agree with the ratios deduced from the second chance plateau in $P_f(A+1)$ and must agree with the ratios deduced from the third chance plateau in $P_f(A+2)$.

B. Compound nucleus formation cross section

The first step in the analysis reported here was the reduction of the cross section data to fission probability accomplished by taking the ratio of the measured cross section to a reaction cross section calculated using the proton optical model parameters of Becchetti and Greenlees.[8] If one ignores direct and pre-compound reactions, this ratio, which was shown in Fig. 5, should closely approximate total fission probability.

The first attempt at applying the rough analysis outlined above produced results which were inconsistent with the branching ratios calculated by others[9] on the basis of empirical systematics. Moreover, the results were self-inconsistent. The Γ_n/Γ_f results for the fissioning nuclei apparently depended strongly on whether the fission was a first, second, or third chance event which

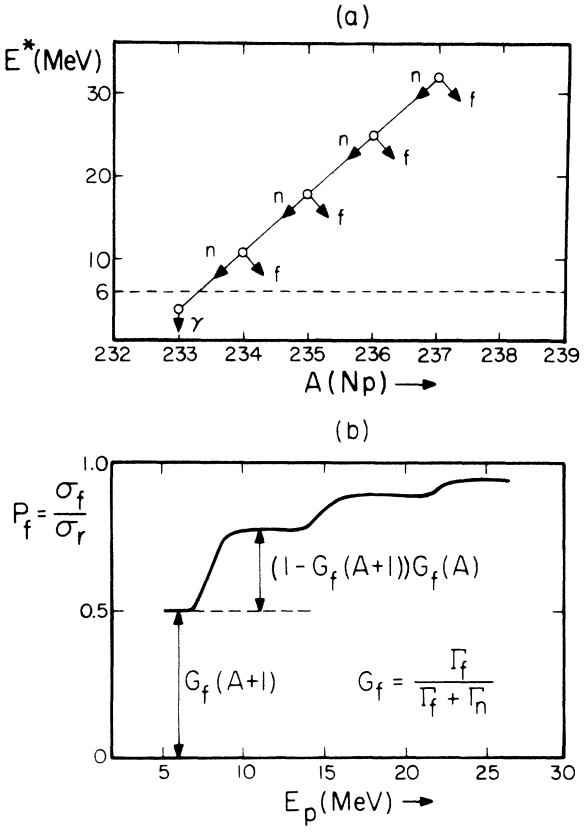

FIG. 6. A schematic representation of proton-induced fission. (a) Reaction path in the $E^*(A)$ vs A plane. (b) Characteristic energy dependence of the fission probability.

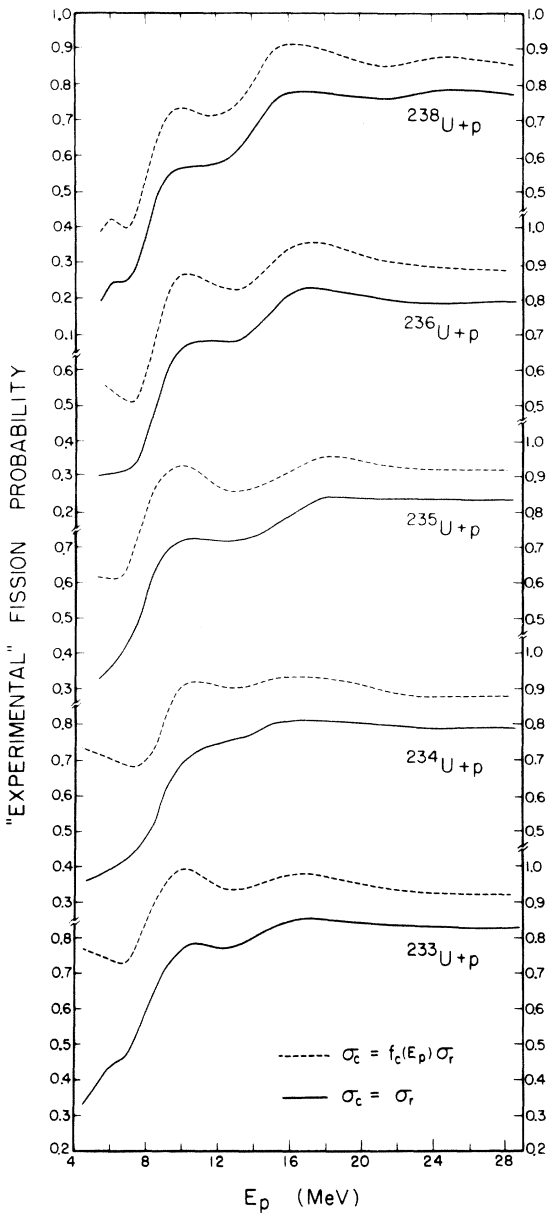

FIG. 7. The effect on the fission probabilities of empirically adjusting the compound nucleus formation cross section as described in the text. The solid lines represent use of an uncorrected optical model reaction cross section and are equivalent to the data shown in Fig. 5. For the dashed lines, the compound nucleus formation cross section is taken to be $\sigma_c = \sigma_r[1.0 - 1.5/E_p - 6.0/E_p^2]$.

contradicts the compound nucleus assumption. In general, the results tended to strongly underestimate first chance fission and overestimate the relative contributions of second and third chance events to the total fission yield.

An explanation of these inconsistencies can be found in the energy dependence of the proton optical model parameters used to compute the reaction cross section. These are the result of a global data search[8] with the relevant data concentrated in the energy regions above the Coulomb barriers. It is not surprising that extrapolation far below the barrier, as in the present case, should be unsatisfactory. Similar conclusions have been reached by Johnson and Kernell[10] in their work with Sn isotopes.

Due to the paucity of available data below the Coulomb barrier, it seemed pointless to embark on a program of varying optical model parameters as functions of energy to obtain better agreement. We have chosen instead to calculate a reaction cross section with the Becchetti and Greenlees parameters[8] and then modify this cross section directly with an energy dependent function to obtain a compound nucleus formation cross section. The boundary conditions for the function chosen were: that it should produce a fission probability for the first chance region reasonably consistent with previously reported systematics; that it should be invariant from isotope to isotope; and finally, the compound nucleus formation cross section should approach the optical model reaction cross section asymptotically for proton energies above the barrier where the optical model parameters are reasonably well determined.

The compound nucleus formation cross section finally used was of the form

$$\sigma_c(E_p) = f_c(E_p)\sigma_r(E_p)\,, \tag{2}$$

with

$$f_c(E_p) = 1.0 + a/E_p + b/E_p^2\,, \tag{3}$$

where E_p is the incident proton energy in MeV and a and b were empirically adjusted constants and σ_r is the reaction cross section obtained from the optical model.

If one assumes the Γ_n/Γ_f is not a rapidly varying function of excitation energy for energy regions well above the necessary thresholds, the constants a and b can be adjusted by comparing the results for neighboring isotopes. This process led to the choice of $a = -1.5$ MeV and $b = -6.0$ MeV^2. The total "experimental" fission probabilities arising from this definition of σ_c are compared with the results of using straight optical model calculations in Fig. 7.

C. Statistical decay model

The calculations undertaken in the second step of the initial analysis presented here are a test of our ability to reproduce the observed fission cross sections using a very simple statistical decay model and assuming standard level density representations for both the ground state and saddle point configurations. The energetics involved in the calculations are demonstrated in Fig. 8. The initial compound nucleus is formed with a formation cross section $\sigma_c(E^*, A+1)$ which can be calculated with the optical model as previously discussed. The excited compound nucleus is then assumed to decay either by neutron emission to a residual state at the ground state deformation or by fission via a saddle point state of intrinsic excitation energy E_s. Charged particle emission is assumed to be strongly suppressed by the Coulomb barrier and Γ_γ, the partial decay width for γ deexcitation is set at 0.03 eV.[11] Fission barriers are assumed to be single peaked and of the inverted harmonic oscillator type.[6]

The first chance fission cross section and the (p,n) cross sections can be written as:

$$\sigma_f^1(p,f) = G_f^1(E^*, A+1)\sigma_c(E^*, A+1)\,, \tag{4}$$

$$\sigma_n^1(p,n_0) = G_n^1(E^*, A+1)\sigma_c(E^*, A+1)\,. \tag{5}$$

The probabilities G_f^1 and G_n^1 are:

$$G_f^1 = \frac{\Gamma_f(E^*, A+1)}{\Gamma_T(E^*, A+1)} = \frac{\Gamma_f}{\Gamma_f + \Gamma_n + \Gamma_\gamma}\,, \tag{6}$$

$$G_n^1 = \frac{\Gamma_n(E^*, A+1)}{\Gamma_T(E^*, A+1)} = \frac{\Gamma_n}{\Gamma_f + \Gamma_n + \Gamma_\gamma}\,. \tag{7}$$

The neutron partial decay width Γ_n was first calculated by Weisskopf[12] as given by

$$\Gamma_n(E^*, A+1) = \frac{1}{2\pi\rho(E^*, A+1)} \times \int_0^{E^*(A+1) - B_n(A+1)} T_n(\epsilon_n)\rho(E^*, A)\,d\epsilon_n\,, \tag{8}$$

where

$$\epsilon_n = E^*(A+1) - B_n(A+1) - E^*(A)\,, \tag{9}$$

$$T_n(\epsilon_n) = \frac{4m_n}{\pi\hbar^2}\,\epsilon_n\sigma_n(\epsilon_n)\,. \tag{10}$$

In this expression ϵ_n is the kinetic energy of the emitted neutron, σ_n is the inverse cross section for a neutron of energy ϵ_n interacting with nucleus (A) at an excitation energy $E^*(A)$, and $\rho(E^*, A+1)$ and $\rho(E^*, A)$ are the level densities of

the two nuclei. The integration is over all available neutron energies. Since neutron cross sections for excited nuclei are generally unavailable, ground state cross sections calculated with the optical model were used. A discussion of the level density formulation used in these calculations can be found in Appendix A.

The fission decay width for the initial compound nucleus is given by

$$\Gamma_f(E^*, A+1) = \frac{1}{2\pi\rho(E^*, A+1)} \times \int_{E_f(A)}^{\infty} T_f(\epsilon_f)\rho(\epsilon_f, A+1)dE_s(A+1), \tag{11}$$

where

$$\epsilon_f = E^*(A+1) - E_s(A+1), \tag{12}$$

$$T_f(\epsilon_f) = [1 + \exp(-2\pi\epsilon_f/h\omega_f)]^{-1}. \tag{13}$$

In these formulas, ϵ_f is the excitation energy of the compound nucleus above the saddle point fission state, $E_f(A+1)$ is the height of the fission barrier, $T_f(\epsilon_f)$ is the Bohr-Wheeler[6] expression for transmission through an inverted harmonic oscillator barrier of circular frequency ω_f, and $\rho(E^*, A+1)$ and $\rho(\epsilon_f, A+1)$ are the appropriate level densities at the ground state and the saddle points. The integration here proceeds over all energetically available saddle point states.

The model can be extended to higher chance fission. For second chance fission we define $P(E^*, A)$ to be the probability that a neutron has been emitted by nucleus $(A+1)$ with energy

$$\epsilon_n = E^*(A+1) - B_n(A+1) - E^*(A), \tag{14}$$

where the residual nucleus (A) has been left with excitation energy $E^*(A)$. Then we have

$$P(E^*, A) = \frac{1}{2\pi\rho(E^*, A+1)} T_n(\epsilon_n)\rho(E^*, A). \tag{15}$$

The residual nucleus (A) can then undergo fission governed by the probability

$$G_f(E^*, A) = \frac{\Gamma_f(E^*, A)}{\Gamma_T(E^*, A)}. \tag{16}$$

The total probability for second chance fission is then the product of (15) and (16) integrated over the statistical energy distribution of the residual nucleus (A):

$$G_f^2(E^*, A+1) = \int_0^{E^*(A+1) - B_n(A+1)} \times P(E^*, A)G_f(E^*, A)dE^*(A). \tag{17}$$

For third chance fission we define $P(E^*, A)$ to be the probability of the first neutron leaving nucleus (A) with excitation energy $E^*(A)$ as defined above. We also define $P(E^*, A-1)$ to be the probability that the second neutron evaporated with energy

$$\epsilon_n = E^*(A) - B_n(A) - E^*(A-1). \tag{18}$$

The probability for third chance fission G_f^3 is the integral over the distribution of energies in the final nucleus $(A-1)$, and over the distribution of energies in the intermediate nucleus (A):

$$G_f^3(E^*, A+1) = \int_0^{E^*(A+1) - B_n(A+1)} P(E^*, A) \int_0^{E^*(A) - B_n(A)} P(E^*, A-1)G_f(E^*, A-1)dE^*(A-1)dE^*(A). \tag{19}$$

Higher chance fission probabilities can be calculated in a similar manner. The total fission probability for the initial compound nucleus $(A+1)$ is the sum of the probabilities $\sum_i G_f^i(A+1)$, $i = 1, 2, 3, \ldots$.

V. RESULTS OF ANALYSIS

A. Application to the data

The most prominent features of the fission probability curves shown in Fig. 5 are the contributions to the total fission probability due to the sequential opening of second and third chance fission channels. Since fourth chance fission apparently contributes little to the data even at the highest energies, our analysis, based on the basic decay scheme outlined in Sec. IV was limited to calculations of the first, second, and third chance processes.

The barrier heights used in the calculations are listed in Table III. The barrier heights for ^{237}Np and ^{238}Np are experimental values. Those for ^{233}Np, ^{234}Np, ^{235}Np, and ^{236}Np were obtained by requiring correspondence between the apparent onset of second chance fission in the calculated and experimental fission probabilities with minor adjustments to optimize agreement between adjacent nuclei [i.e., third chance threshold for the $(A+1)$ nucleus and the first chance level for the $(A-1)$ nucleus]. The necessity for these adjustments demonstrates the added constraint provided by sequential target isotopes.

Total fission probabilities calculated with averaged Gilbert and Cameron parameters (Appendix

A) are compared with the data in Fig. 9. It is apparent that the agreement with the data is poor, both as to energy dependence and magnitude. In general, fission probabilities are underestimated and tend to decrease much too rapidly as excitation energy increases.

Shown in Fig. 10 are calculations where the shell corrections given by Gilbert and Cameron were arbitrarily decreased by 0.75 MeV for the saddle point decay. The same shell corrections are used for all nuclei. These corrections produce level density parameters for the two decay channels whose ration a_f/a_n is about 1.06. The agreement with the data is improved, particularly with regard to the energy dependence.

Major discrepancies still exist, particularly for second chance fission for $^{236}U+p$ and for $^{238}U+p$. Within the framework of the present analysis major uncertainties are introduced by the use of optical model results for σ_c and for the inverse neutron cross sections σ_n used in the neutron branch calculations. The compound nucleus formation cross section σ_c has been discussed previously. A comparison of neutron values calculated for neighboring nuclei for which experimental data are available[13] indicates that the uncertainty in σ_n could be as much as a factor of 2 for neutron energy regions important to our fission probability calculations. Generally, our optical model calculations of σ_n using the Becchetti and Greenlees parameters[8] are in reasonable agreement with available neutron data for those actinide nuclei which undergo thermal fission; however, the optical model results are in serious disagreement with existing data sets[13] for actinide nuclei which do not fission thermally, particularly with regard to the energy dependence of the cross sections for neutron energies below about 8 MeV. A discrepancy in this cross section can introduce considerable error into the calculations of Γ_n, particularly in the case of the second chance fis-

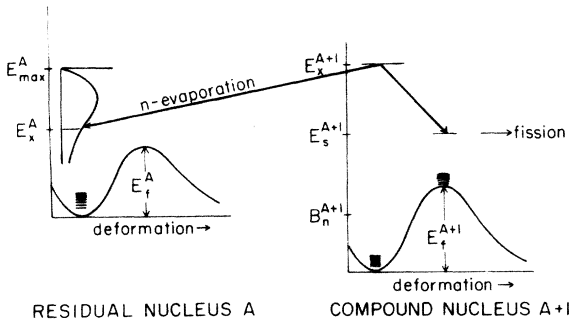

FIG. 8. A schematic of the decay scheme used in the statistical model formulation.

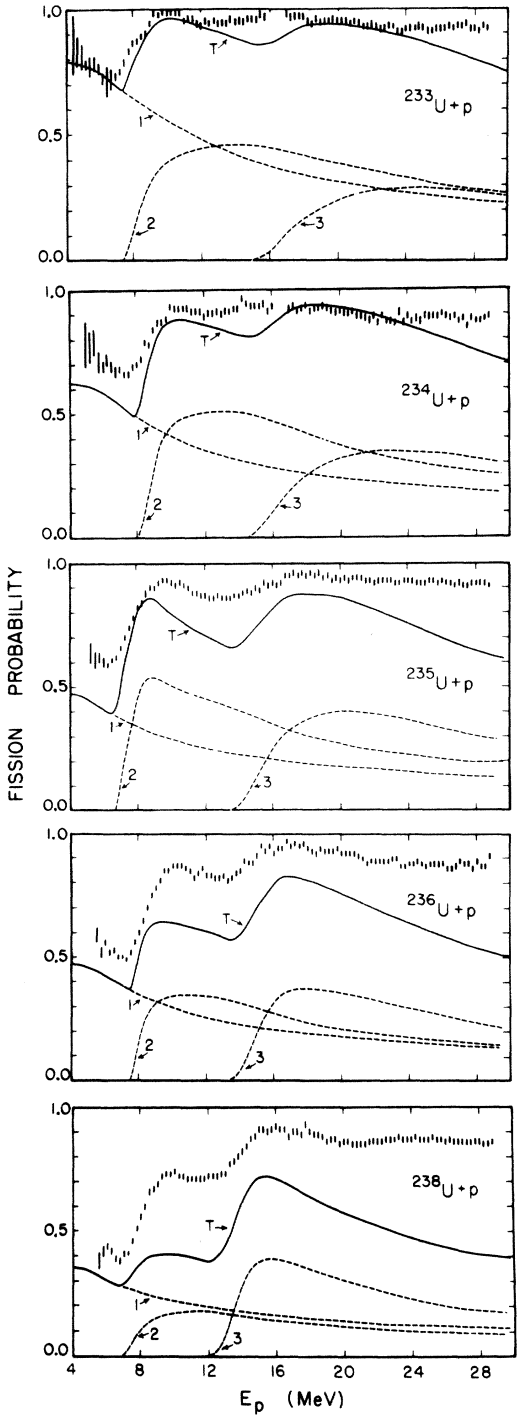

FIG. 9. Fission probabilities calculated using averaged Gilbert and Cameron (Ref. 7) level density parameters for both the ground state and the saddle point deformation. The experimental data are obtained with the adjusted compound nucleus formation cross section. Curves labeled 1, 2, 3, and T refer to first chance, second chance, third chance, and total fission probability, respectively.

sion branch for $^{238}U + p$ and to a lesser extent for second chance fission of $^{236}U + p$. Until these fundamental uncertainties are reduced it was felt that further parameter variation to produce a better fit would have little significance.

B. Branching ratios

Branching ratios resulting from the calculations shown in Fig. 10 are shown in Fig. 11. Ratios shown are constrained by fits to at least two excitation curves and therefore should be less dependent on possible errors in σ_c. The nonuniform behavior evident for $(E^* - B_n)$ about 2.5 MeV is artificial and occurs because the transition point between a constant temperature form to a Fermi gas form for the Gilbert and Cameron level densities takes place at different excitation energies in the initial nucleus for the neutron and fission branches. In general, these ratios show their expected increase with decreasing fissionability of the nucleus. The present calculations show Γ_n/Γ_f ratios increasing with A and for the energy region $E_p = 10$ to 25 MeV our results are relatively constant.

In Fig. 12 these ratios are plotted vs $(E_f - B_n)$ for an excitation energy of 15 MeV for two different assumptions regarding the level densities. In Fig. 12(a), averaged Gilbert and Cameron parameters are used for both neutron and fission channels, while Fig. 12(b) shows the effect of reducing shell corrections in the fission channel. These figures are taken from the calculations shown in Figs. 9 and 10, respectively. On the right hand side of each figure, the Γ_n/Γ_f ratios are plotted as functions of $(E_f' - B_n')$, where $E_f' = E_f + P_f$ and $B_n' = B_n + P_n$ are the effective fission barriers and effective neutron binding energies when pairing effects are included. The absolute values of the Γ_n/Γ_f ratios may be in error by as much as a factor of 2 due to the uncertainties introduced by the optical model calculations. However, their relative values should not be appreciably affected by such errors.

Table IV tabulates the relative contributions to the total fission yield from first, second, and third chance fission. The sizable contribution from at least second chance fission at relatively low proton energies indicates the necessity to consider the effect of these channels in accurate fission studies. The average excitation energy difference between a first and second chance fission event is approximately 6 to 7 MeV for the actinide region, a difference which can be highly significant in many studies.

C. Discussion

The analysis presented thus far has obviously ignored many effects which are expected to be

TABLE III. Table of energies in MeV.

Neptunium isotope	Binding energies B_p (Ref. a)	B_n (Ref. a)	Barrier heights E_f (Ref. b)	(Ref. c)
239	5.298	6.227	5.553	5.30
238	...	5.480	6.05	6.05
237	4.860	6.619	5.49	5.50
236	4.786	5.691	6.175	5.60 ± 0.25
235	4.400	6.991	5.415	5.60 ± 0.18
234	4.250	6.120	5.995	5.40 ± 0.20
233	...	7.350	5.147	5.40 ± 0.23
232	...	6.410	5.649	5.50

[a] All binding energies were obtained from A. H. Wapstra and N. B. Gove [Nucl. Data A9, 265 (1971)].

[b] All values are from V. E. Viola, Jr., and B. D. Wilkins [Nucl. Phys. 82, 65 (1966)] and are theoretical except for ^{238}Np and ^{237}Np which are experimental (see E. K. Hyde, *The Nuclear Properties of the Heavy Elements* (Prentice-Hall, Englewood Cliffs, N.J., 1964), Vol. III, p. 23.

[c] Results of this work. Uncertainties quoted for fission thresholds are the result of a χ^2 minimization for the region of second chance fission threshold. The value given for ^{239}Np is estimated only from the first chance plateau and thus depends critically on the choice of σ_c for this region.

TABLE IV. Relative contribution of consecutive fission decay channels to total fission yield.

Target	E_p (MeV)	P_f^1/P_F	P_f^2/P_F	P_f^3/P_F
^{233}U	5	1.00	...	...
	10	0.68	0.32	...
	15	0.65	0.35	...
	20	0.62	0.33	0.05
^{234}U	5	1.00	...	...
	10	0.65	0.35	...
	15	0.60	0.40	...
	20	0.57	0.36	0.07
^{235}U	5	1.00	...	...
	10	0.64	0.36	...
	15	0.57	0.34	0.09
	20	0.51	0.30	0.19
^{236}U	5	1.00	...	...
	10	0.56	0.44	...
	15	0.50	0.40	0.10
	20	0.48	0.32	0.20
^{238}U	5	1.00	...	...
	10	0.55	0.45	...
	15	0.43	0.37	0.20
	20	0.45	0.34	0.21

$P_F = \sum_i P_f^i$, the total fission probability

important in a definitive treatment of the sequential decay process at high excitation energies. Among those which have been investigated but not included are the following:

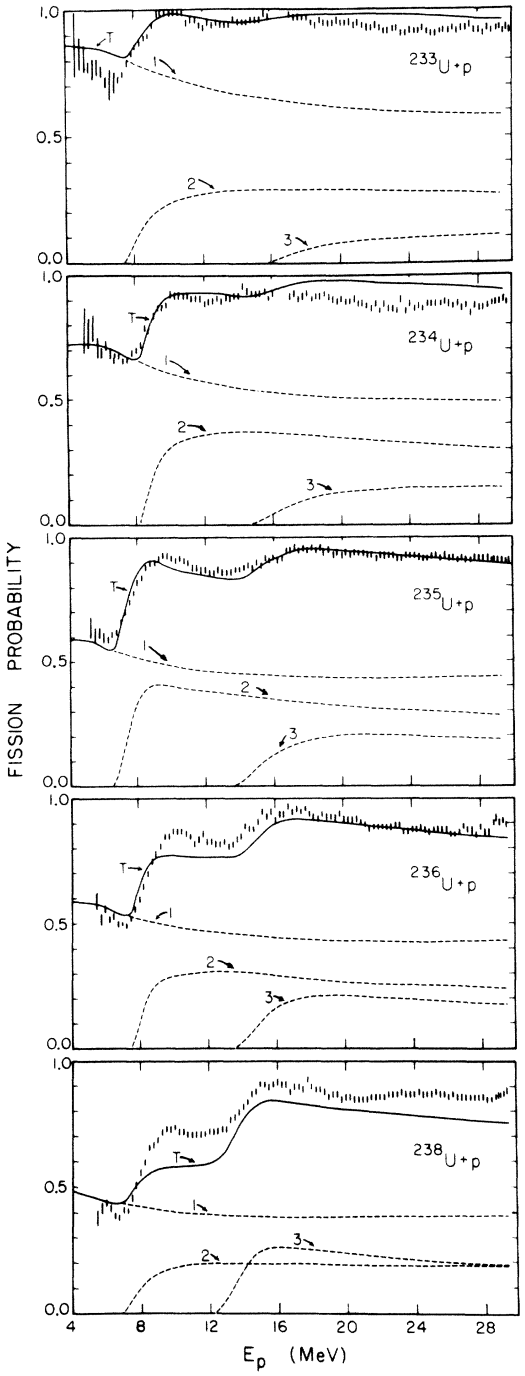

FIG. 10. Fission probabilities calculated using adjusted shell corrections in the level density prescription. These shell corrections are approximately equivalent to $a_f/a_n = 1.06$.

1. *Fourth chance fission*

The most obvious of these processes is fourth chance fission, occurring after the emission of three neutrons. Presence of fourth chance fission events is evident in the $^{238}U + p$ and $^{235}U + p$. Omission of this channel from the calculation should lead to underestimates of total fission probability for the higher A targets with the effect decreasing with A.

2. *Angular momentum effects*

We have used the spin zero level density formalism and have ignored angular momentum effects in the calculations. Qualitatively, inclusion of the spin dependence in the calculations would tend to increase the fission yields at the higher excitation energies as a consequence of the higher average angular momenta involved. Within the scope of this statistical model, the dependence of Γ_n/Γ_f on J is approximately given by

$$(\Gamma_n/\Gamma_f)_J = (\Gamma_n/\Gamma_f)_0 \exp\left[-\left(\frac{1}{2\sigma_n^2} - \frac{1}{2\sigma_f^2}\right) J(J+1)\right], \tag{20}$$

where the σ_n and σ_f are the spin cutoff parameters for neutron emission and fission, respectively. On the assumption that $\sigma_f^2 = 2\sigma_n^2$ the actual effect upon Γ_n/Γ_f should be considerably less than 10% at $E_p = 30$ MeV.

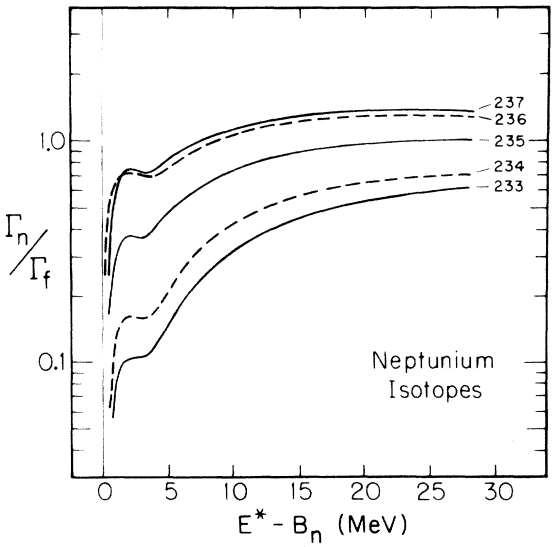

FIG. 11. The Γ_n/Γ_f ratios taken from the fission probability calculations of Fig. 10. Above the threshold region they change quite slowly with excitation energy.

3. *Charged particle emission*

The model does not include charged particle emission. For proton energies above the Coulomb barrier charged particle emission may make a contribution to the total reaction cross section and would tend to reduce the calculated fission probabilities by a few percent.

4. *Pre-equilibrium decay (Ref. 14)*

Another effect to be considered is that of pre-equilibrium decay of the compound nucleus. For estimates of this effect we are indebted to calculations performed at Rochester by Blann.[15] The situation presented by pre-equilibrium decay of the compound nucleus is graphically portrayed in Fig. 13. The neutron energy spectrum resulting from this type of emission is much less strongly peaked at low energies than that from statistical decay of the compound nucleus. Very significant neutron yields persist out to neutron energies which would leave the initial nucleus at quite low excitations. The net effect would be to reduce the fission yields at energies above about 20 MeV where pre-equilibrium decay begins to have an appreciable cross section. It is primarily this process which is responsible for the "saturation" of total fission probability at values between 80 and 90% rather than close to 100% as would be expected on standard statistical grounds.

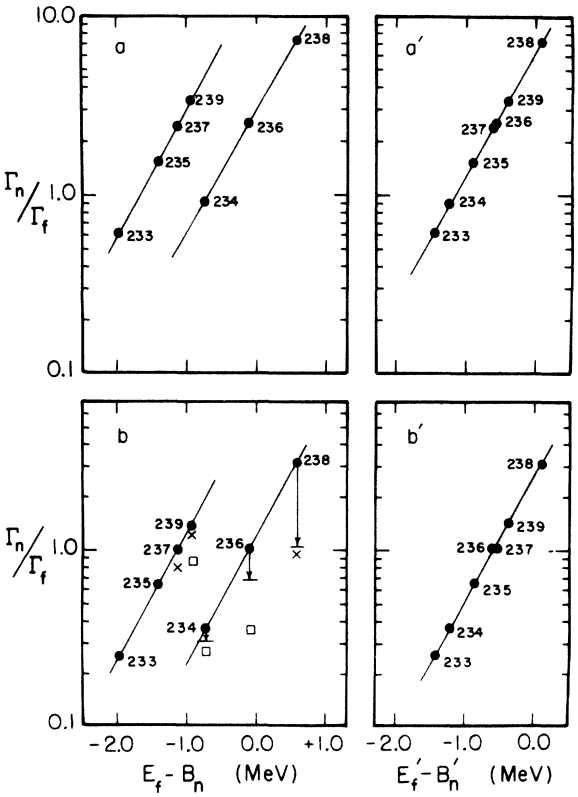

FIG. 12. Branching ratios for the neptunium isotopes at an excitation energy of 15 MeV. The two sets shown in (a) and (b) correspond to the probability calculations shown in Figs. 9 and 10. Arrows indicate Γ_n/Γ_f values which would be required by the data in those cases for which the calculation of Fig. 10 failed to approximate the observed fission probabilities. Squares refer to values reported in Ref. 9 for $^{239.5}$Np, ^{236}Np, and ^{234}Np at approximate excitation energies of 13, 18, and 18 MeV, respectively. The values shown by x's for ^{239}Np, ^{238}Np, and ^{237}Np are from Ref. 5 for excitation energies of 17, 17, and 15 MeV, respectively.

Each of these effects would contribute a small amount to the total yield. They do not appreciably affect the data and their inclusion would not affect the analysis for $E_p < 18$ MeV.

A rigorous treatment of the compound decay process should include the effect of compound fission barriers and possibly deformation dependent level density formalisms[16] for neutron emission and fission decay. However inclusion of these effects probably will not be particularly fruitful until the previously discussed uncertainties in σ_c and σ_n are resolved.

VI. CONCLUSIONS

A series of very accurate measurements of cross sections for proton induced fission of the uranium isotopes has been presented. It has been demonstrated that, when Coulomb penetrability effects are removed from the excitation curves, threshold effects associated with multichance fission are revealed and previously unreported fission barrier heights may be estimated. Because the data cover a wide range of proton energies and a sequence of target isotopes an analysis is possible which allows determination of relative Γ_n/Γ_f ratios for the sequence of isotopes involved. In addition the relative contributions to the total fission can be determined.

The simple statistical decay model used in the analysis can be improved by inclusion of various well known effects. However, the absolute accuracy with which the Γ_n/Γ_f ratios can be determined is limited by basic uncertainties introduced by the use of optical model cross sections in the analysis. Resolving this problem would permit a much more accurate study of the effect of excitation energy upon the fission process.

APPENDIX A

The principal thrust in recent level density calculations for the fission process has been to develop microscopic calculations for deformed nuclear shapes.[17] We have not chosen this route

but have chosen to use the empirically based Gilbert and Cameron prescription[7] for both the particle emission process and the saddle point transition. To reduce computation times required, a further simplification of the calculation was made by using the spin zero formulation.

The spin zero case is given by:

$$\rho(E,A) = \begin{cases} \dfrac{\exp[(E-E_0)/T]}{2T\sigma^2}, & \text{for } E < E_x, \\ \dfrac{\exp[2(aU)^{1/2}]}{(2)^{5/2}a^{1/4}U^{5/4}\sigma^3}, & \text{for } E > E_x, \end{cases} \tag{21}$$

where

$$E_x = U_x + P = U_x + [P(Z) + P(N)], \tag{22}$$

$$U_x = 2.5 + 150.0/A, \tag{23}$$

$$U = E - P = E - [P(Z) + P(N)], \tag{24}$$

$$\sigma^2 = \begin{cases} 0.0888(aU_x)^{1/2}A^{2/3}, & \text{for } E < E_x, \\ 0.0888(aU)^{1/2}A^{2/3}, & \text{for } E > E_x, \end{cases} \tag{25}$$

$$a/A = 0.00917[S(Z) + S(N)] + 0.120. \tag{26}$$

For the initial calculation, average values of the shell corrections $S(Z)$ and $S(N)$ and pairing energies $P(Z)$ and $P(N)$ were used rather than allowing them to vary with A as given by Gilbert and Cameron. In view of the large deformations present, this seemed a more realistic approach than accepting the ground state variations given by Gilbert and Cameron at face value. In the later calculations shell corrections for the neutron channel and fission channel were set at $S_n = [S(N) + S(Z)]_n = -0.18$ MeV and $S_f = [S(N) + S(Z)]_f = +0.57$ MeV, respectively.

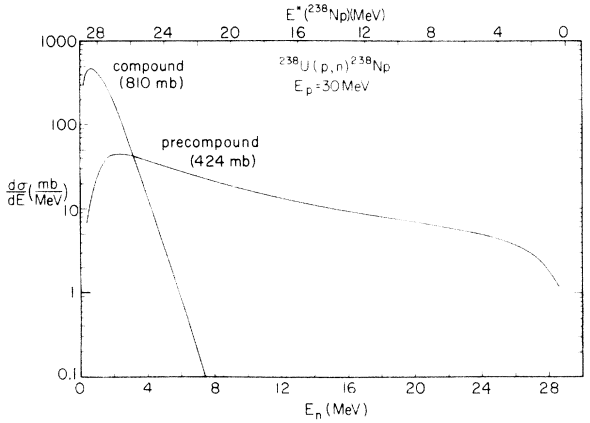

FIG. 13. Relative contributions of compound decay and pre-compound decay to the neutron spectrum for $^{238}U(p,n)^{238}Np$ at $E_p = 30.0$ MeV. It can be seen that the integrated pre-compound yield is a significant factor at this energy.

*Work supported in part by a grant from the Shell Oil Companies, Incorporated. Most of this work along with a tabulation of the fission cross sections is contained in the Ph.D. dissertation of J. R. Boyce, Duke University, 1972 (unpublished).

†Present address: Los Alamos Scientific Laboratory, Los Alamos, New Mexico 87544.

‡On leave from: Institut fur Kernphysik der Universitat, Frankfurt, West Germany.

§Work supported in part by the U. S. Atomic Energy Commission.

¶Work supported in part by the U. S. Atomic Energy Commission under contract with Union Carbide Corporation.

[1]C. B. Fulmer, Phys. Rev. 116, 418 (1959).

[2]G. R. Choppin, J. R. Meriwether, and J. D. Fox, Phys. Rev. 131, 2149 (1963).

[3]G. L. Bate and J. R. Huizenga, Phys. Rev. 133, B1471 (1964).

[4]S. Baba, H. Umezawa, and H. Baba, Nucl. Phys. A175, 177 (1971).

[5]C. J. Bishop, I. Halpern, R. W. Shaw, Jr., and R. Vandenbosch, Nucl. Phys. A198, 161 (1972).

[6]N. Bohr and J. A. Wheeler, Phys. Rev. 56, 426 (1939).

[7]A. Gilbert and A. G. W. Cameron, Can. J. Phys. 43, 144 (1965).

[8]F. D. Becchetti and G. W. Greenlees, Phys. Rev. 182, 1190 (1969).

[9]R. Vandenbosch and J. R. Huizenga, in *Proceedings of the Second United Nations International Conference on the Peaceful Uses of Atomic Energy, Geneva, 1958* (United Nations, Geneva, Switzerland, 1958), Vol. 15, p. 248; J. R. Huizenga *et al.*, Phys. Rev. 126, 210 (1962).

[10]C. H. Johnson and R. L. Kernell, Phys. Rev. C 2, 639 (1970).

[11]J. E. Lynn, *The Theory of Neutron Resonance Reactions* (Clarendon, Oxford, 1968), p. 316.

[12]V. F. Weisskopf, Phys. Rev. 52, 295 (1937).

[13]J. J. Schmidt, Kernforschungszentrum Karlsruhe Report No. KFK 120 (EANDC-E-35), December, 1962 (unpublished).

[14]M. Blann and F. M. L. Lanzafance, Nucl. Phys. A142, 559 (1970).

[15]M. Blann, University of Rochester, private communications.

[16]H. C. Britt, M. Bolsterli, J. R. Nix, and J. L. Norton, Phys. Rev. C 7, 801 (1973).

[17]J. R. Huizenga and L. G. Moretto, in *Annual Reviews of Nuclear Science*, edited by E. Segrè (Annual Reviews, Palo Alto, California, 1972) Vol. 22, p. 427.